

Cold-gas outflows in typical low-redshift galaxies are driven by star formation, not AGN

Marc Sarzi^{1*}, Sugata Kaviraj¹, Borislav Nedelchev¹, Joshua Tiffany², Stanislav S. Shabala³, Adam T. Deller⁴ and Enno Middelberg⁵

¹Centre for Astrophysics Research, University of Hertfordshire, College Lane, Hatfield AL10 9AB, United Kingdom

²Astronomy Unit, School of Physics and Astronomy, Queen Mary University of London, London E1 4NS, UK

³School of Mathematics and Physics, University of Tasmania, Private Bag 37, Hobart, TAS 7001, Australia

⁴The Netherlands Institute for Radio Astronomy (ASTRON), Dwingeloo, The Netherlands

⁵Astronomisches Institut der Ruhr-Universität Bochum, Universitätsstrae 150, D-44801 Bochum, Germany

7 March 2022

ABSTRACT

Energetic feedback from active galactic nuclei (AGN) is an important ingredient for regulating the star-formation history of galaxies in models of galaxy formation, which makes it important to study how AGN feedback actually occurs in practice. In order to catch AGNs in the act of quenching star formation we have used the interstellar Na I $\lambda\lambda$ 5890, 5895 (NaD) absorption lines to look for cold-gas outflows in a sample of 456 nearby galaxies for which we could unambiguously ascertain the presence of radio AGN activity, thanks to radio imaging at milli-arcsecond scales. While compact radio emission indicating a radio AGN was found in 103 galaxies (23% of the sample), and 23 objects (5%) exhibited NaD absorption-line kinematics suggestive of cold-gas outflows, not one object showed evidence of a radio AGN and of a cold-gas outflow simultaneously. Radio AGN activity was found predominantly in early-type galaxies, while cold-gas outflows were mainly seen in spiral galaxies with central star-formation or composite star-formation/AGN activity. Optical AGNs also do not seem capable of driving galactic winds in our sample. Our work adds to a picture of the low-redshift Universe where cold-gas outflows in massive galaxies are generally driven by star formation and where radio-AGN activity occurs most often in systems in which the gas reservoir has already been significantly depleted.

Key words: galaxies: elliptical and lenticular, cD – galaxies: spiral – galaxies: nuclei – galaxies : evolution

1 INTRODUCTION

Understanding the processes that quench star formation activity is key to following how galaxies evolve over cosmic time. In massive galaxies, which have deep potential wells, the current view is that stellar winds and supernovae explosions are not powerful enough to eject gas and regulate star formation (e.g., Silk & Rees 1998). Instead, this quenching is typically attributed to a central active galactic nucleus (AGN, e.g., Croton et al. 2006; Shabala & Alexander 2009), because the energy released by the growth of the black hole can be orders of magnitude larger than the binding energy of the gas, even in the most massive systems (e.g., Fabian 2012). Observational evidence for this process remains mixed, however. While some examples of AGN-driven outflows do exist both at high and low redshifts (e.g., Nesvadba et al. 2008; Nyland et al. 2013, respectively), it is unclear whether gas outflows are routinely driven by AGNs. In particular, recent work at low redshift indi-

cates that the onset of the AGN appears to lag behind the peak of the starburst by several dynamical timescales (Kaviraj 2009; Wild, Heckman & Charlot 2010; Shabala et al. 2012; Kaviraj et al. 2015b), which implies that the gas reservoir has been significantly depleted before the AGN had a chance to couple to it. To probe this issue in more detail, it is desirable to investigate whether signatures of cold-gas outflows exist in systems that host optical or radio AGNs and to see how these outflows compare to those in star-bursting systems.

An effective way of carrying out this exercise is to explore the presence of interstellar Na I $\lambda\lambda$ 5890, 5895 (NaD) absorption in nearby galaxies. When outflows occur in galaxies, neutral material entrained in the flow can be observed against the stellar background via characteristic absorption lines (e.g., Rupke, Veilleux, & Sanders 2005; Sato et al. 2009; Chen et al. 2010), particularly in systems with low inclination. At optical wavelengths, the strongest of such absorption lines are produced by neutral Sodium and observed via the NaD doublet. Thus, if AGN feedback routinely shuts down star formation by driving cold-

* E-mail: m.sarzi@herts.ac.uk

Morph. / em.-line class	all objects		mJIVE-20 det.	
	all	with NaD	all	with NaD
ETG / SF	19	6	1	0
ETG / TO	15	6	4	1
ETG / Sy	19	4	3	0
ETG / LI	9	4	5	2
ETG / NE	204	42	80	15
LTG / SF	69	29	0	0
LTG / TO	46	26	2	0
LTG / Sy	26	9	1	0
LTG / LI	9	3	3	1
LTG / NE	27	16	0	0
Merger / SF	4	1	0	0
Merger / TO	0	0	0	0
Merger / Sy	3	0	2	0
Merger / LI	2	0	1	0
Merger / NE	4	2	1	1

Table 1. Breakdown of our sample according to galaxy morphology and nebular emission classification (where NE stands for objects with little or no emission), for all our objects and those with a VLBI radio core, as well as for those with detected NaD excess.

gas outflows, one expects to find an excess of NaD absorption over what is expected from stellar photospheres alone, which is blueshifted compared to the position of the photospheric NaD lines.

In this Letter, we use optical spectra from the Sloan Digital Sky Survey (SDSS, Abazajian et al. 2009) to investigate the NaD properties of a sample of galaxies that have been observed by the mJy Imaging VLBA Exploration at 20 cm survey (Deller & Middelberg 2014, hereafter mJIVE-20). While SDSS spectra enable us to identify optical AGNs, the sub-arcsecond radio imaging obtained with the Very Long Baseline Array (VLBA) during the mJIVE-20 survey allows us to unequivocally identify the presence of radio AGN activity. Taken together, these data enable a detailed exploration of whether AGN are an important driver of outflows in the massive galaxy population.

This paper is organised as follows. In § 2 we describe our sample together with the mJIVE-20 survey and SDSS data that underpin this study, whereas § 3 describes our analysis of the NaD absorption lines. In § 4 we then scrutinise the kinematics of the NaD lines to robustly identify objects with interstellar NaD absorption and look for evidence for starburst- or AGN-driven cold-gas outflows. Finally, we draw our conclusions in § 5.

2 SAMPLE AND DATA

Our sample comprises of galaxies observed during the mJIVE-20 survey for which images and spectra are available from the SDSS. mJIVE-20 is a survey that systematically observed objects detected by the Faint Images of the Radio Sky at Twenty cm (FIRST, Becker, White & Helfand 1995), with a median detection threshold of 1.2 mJy/beam and a typical beam size of $\sim 0''.01$ that effectively allows to zoom in on the FIRST targets to further study the nature of the radio emission and ascertain in particular the presence of a radio core associated with an AGN. The mJIVE-20 survey has targeted $\sim 25,000$ FIRST sources, with ~ 5000 very-long baseline interferometry (VLBI) detections.

We cross-matched the mJIVE-20 targets with the DR7 value-

added SDSS catalogue of Oh et al. (2011, hereafter OSSY), since this contains spectral measurements for the stellar kinematics and the nebular emission within the $3''$ SDSS fiber. Based on pPXF and GandALF fits (Cappellari & Emsellem 2004; Sarzi et al. 2006), the OSSY catalogue also provides us with a measurement for the level of detection of the emission lines through their A/N ratio, between the peak amplitude of the lines and noise level in the GandALF fit residuals, and a gauge for the amount of dust extinction that affects the entire SDSS spectrum. Such a diffuse E(B-V) measurement is particularly relevant to this work, since it corresponds well to the presence of interstellar NaD absorption (Jeong et al. 2013). The OSSY database also readily provides us with the best-fitting model for the stellar continuum, which is central to correctly characterise the extent and kinematics of interstellar NaD absorption. Finally, the OSSY catalogue is restricted to targets at $z < 0.2$ so that a robust visual classification of the galaxy morphology is possible.

Overall, our sample includes 456 galaxies with a median stellar mass of $10^{11} M_{\odot}$. Of these, 58% are early-type galaxies (ETGs), 39% are spirals (LTGs) and 3% are on-going mergers. Approximately 23% of our sample (103 galaxies) have VLBI detections, 90% of which occur in ETGs. Tab. 1 provides a breakdown of our sample according to galaxy morphology and to whether they have a VLBI radio core.

3 SPECTRAL ANALYSIS

In order to assess the presence of interstellar NaD absorption and measure the kinematics of such absorbing clouds, we follow the approach of Rupke, Veilleux, & Sanders (2005) after normalising the SDSS spectra for the best-fitting stellar continuum provided by the OSSY catalogue. We assume a single Maxwellian velocity distribution for the absorbers along the line of sight and that the covering fraction C_f of such clouds is itself independent of velocity. Under these assumptions the absorption profile of the interstellar NaD lines can be written as

$$I(\lambda) = 1 - C_f \left\{ 1 - \exp \left[- 2\tau_0 e^{-(\lambda - \lambda_{\text{blue}})^2 / (\lambda_{\text{blue}} b/c)^2} - \tau_0 e^{-(\lambda - \lambda_{\text{red}})^2 / (\lambda_{\text{red}} b/c)^2} \right] \right\} \quad (1)$$

where λ_{blue} and λ_{red} are the redshifted central wavelength of the Na I doublet, τ_0 is the optical depth at the centre of the red line, and $b = \sqrt{2}\sigma$ is the Doppler parameter that measures the width of the lines. This parametrisation thus yield a measurement for the velocity V_{NaD} and width σ_{NaD} of the NaD lines, as well as the optical depth τ_0 and covering factor C_f of the absorbing clouds.

After normalising the SDSS spectra of our sample galaxies for the OSSY continuum model we proceed to fit with the Rupke, Veilleux, & Sanders method any possible excess of NaD absorption in the data compared to what is expected from the photospheric absorption provided by the OSSY best fitting stellar-population model. Our approach implicitly assumes that any NaD absorption excess is due to interstellar absorption but in fact this is not always the case. Indeed, ETGs showing little or no dust absorption in their images or nebular emission in their spectra often exhibit an NaD excess that is most likely due to an enhanced [Na/Fe] abundance in their stellar populations that cannot be accounted for by most stellar population models (Jeong et al. 2013), in particular given that in such smooth and ordinary ETGs the NaD excess shows little or no kinematic offset compared to the systemic velocity (Park, Jeong and Yi 2015). However, in what follows, we

will show that objects where the NaD excess stems from template mismatch can be clearly isolated in terms of both the position and width of their best-fitted NaD profile in addition to their reddening and nebular properties.

Fig. 1 shows SDSS colour images and our spectral fit in the NaD region for five galaxies in our sample, all of which display a significant excess of NaD absorption compared to the photospheric NaD absorption of the best-fitting stellar-population model (i.e., the A/N ratio for the fitted NaD profile is < -3). Fig. 1 also indicates the different nature of the NaD absorption excess between spiral or dusty ETGs and quiescent objects. Indeed, whereas in spiral galaxies and dust-lane ellipticals our fit returns narrow NaD profiles that can be either blue- or even slightly redshifted (first four panels from the left), the NaD excess of quiescent ETGs (rightmost panel) is generally characterised by rather broad NaD model profiles. Tab. 1 also specifies where NaD excess occurs in our sample.

4 RESULTS

4.1 Entire Sample

We begin by discussing the emission-line classification and, where present, the properties of the NaD excess for our entire sample. Fig. 2 (left panel) shows the standard Baldwin, Phillips & Terlevich (1981, BPT) diagnostic diagram that juxtaposes the $[\text{O III}]/\text{H}\beta$ and $[\text{N II}]/\text{H}\alpha$ line ratios (Veilleux & Osterbrock 1987) for objects with $A/N > 3$ for all four lines, from which we deduce their emission-line class. Of the 221 objects that are in this BPT diagram, which are nearly 48% of the sample (see also Tab. 1), most show emission either dominated by star-forming regions (hereafter SF, 42% of active objects) or by the likely superposition of star-bursting and AGN activity (TO for “transition objects”, 28%), with the remaining objects exhibiting either Seyfert activity (Sy, 22%) or central LINER emission (LI, 9%). The remaining 235 objects in our sample (nearly 52%) display only weak (e.g., with only $\text{H}\alpha$ and $[\text{N II}]$ detected emission) or no nebular emission, which is puzzling considering that only 1/3 of these objects show a compact radio core at VLBI resolution so that radio AGN activity could account for their FIRST radio flux. On the other hand, since 87% of such quiescent or weakly emitting objects are ETGs, it is likely that for many of those without a VLBI detection the FIRST radio flux is due to circumnuclear or rather extended star-formation activity, which would add to existing evidence of recent star-formation in many ETGs based on UV imaging (e.g., Yi et al. 2005; Jeong et al. 2007).

Moving on with the properties of the NaD absorption excess for our entire sample, the middle and right panels of Fig. 2 show - for objects where such an absorption excess is detected - how the position and width of our best-fitting NaD profile compares to that of the stellar line-of-sight velocity distribution. In these $V_{\text{NaD}} - V_{\text{stars}}$ vs. $\sigma_{\text{NaD}} - \sigma_{\text{stars}}$ diagrams we can identify objects with a) possible NaD outflows where $\Delta V \lesssim -100 \text{ km s}^{-1}$, b) relaxed dusty disks where $\Delta V \sim 0$ but $\Delta\sigma < 0$, corresponding to narrower NaD interstellar absorption lines compared to stellar photospheric features, c) possible mild inflows due to bars or unsettled dust lanes where $\Delta\sigma < 0$ and $\Delta V > 0$, and finally d) systems that systematically show $\Delta\sigma > 0$, $\Delta V \sim 0$ and no evidence for an interstellar medium as their GandALF fits imply little or no need for reddening by dust (Fig. 2, right panel) and only weak or no nebular emission. The NaD excess of these last objects is almost certainly due to template-mismatch, where the large width of such an excess is likely driven by an enhanced presence of cool stars and the strong pressure-broadened wings of their NaD photospheric lines.

There are 23 objects with possible NaD outflows in our sample, most of which (74%) exhibit either SF or TO central activity, consistent with SDSS studies on starburst-driven outflows (e.g., Chen et al. 2010) and possibly with an evolution from starburst to quenched galaxies with star formation decreasing along this path as AGN emerge (e.g., Yesuf et al. 2014), respectively. On the other hand, there is little evidence for NaD outflows in galaxies harbouring Seyfert nuclei or LINER emission. The few objects with little or no nebular emission that show evidence of NaD outflow in Fig. 2 (including a spectacular case with $\Delta V \sim -1000 \text{ km s}^{-1}$ shown by the left-pointing arrow) are most likely SF or TO where the $[\text{O III}]$ line remained undetected due to large amounts of reddening.

4.2 mJIVE-20 Detected Objects

Around 23% of our FIRST-selected sample of galaxies (103 objects) show unequivocal signatures of AGN activity through to the detection of a compact radio core in the mJIVE-20 images. These are generally (79% of the cases) objects that show only weak or no nebular emission, or which are otherwise evenly distributed between the regions of the $[\text{O III}]/\text{H}\beta$ vs. $[\text{N II}]/\text{H}\alpha$ BPT diagram that include transition objects, Seyfert nuclei and galaxies with LINER emission, consistent with the presence of an AGN as signalled by the finding of a compact radio core. In fact, central SF activity in our VLBI-detected objects is likely to be rather limited given that most of their FIRST flux is unresolved (90 objects have more than 80% of their total FIRST flux density in an unresolved component) and that generally (86 objects, or 83%) more than half of this compact emission is found in the VLBI component. Furthermore, VLBI-detected galaxies reside primarily on the red-sequence of passively-evolving system in the UV-optical color-magnitude diagram (Kaviraj et al. 2015a), which is sensitive to even small fractions of young stars (Yi et al. 2005; Kaviraj et al. 2007).

Among the VLBI-detected objects, 20 ($\sim 19\%$) show an NaD absorption excess, and these are predominantly ETGs with little or weak nebular emission (Fig. 3). For a third of these galaxies, however, such an excess is most likely induced by template-mismatch given their position in the $V_{\text{NaD}} - V_{\text{stars}}$ vs. $\sigma_{\text{NaD}} - \sigma_{\text{stars}}$ diagram and their lack of reddening by dust. The remaining objects, a dozen at best, show no evidence of outflows and are instead consistent with the presence of relaxed dusty disks or slight inflows, possibly indicating unsettled dust-lanes. Thus, only a minority of nearby radio AGN is found in galaxies where NaD absorption indicates the presence of cold-gas, and in no systems do we find evidence for such a medium to be outflowing.

This result contrasts with the findings of Lehnert et al. (2011), who detected an NaD excess in approximately 1/3 of their sample of radio-loud ETGs and with NaD profiles showing little or no kinematic offset ($\Delta V \sim -50 \text{ km s}^{-1}$) but very broad profiles ($\sigma_{\text{NaD}} \sim 500 \text{ km s}^{-1}$). Part of this discrepancy may be due to differences in sample selection. Lehnert et al. analysed a sample of 700 radio-loud ETGs at $z < 0.2$, with FIRST 1.4 GHz flux densities above 40 mJy and resolved jet morphologies. This selection would naturally sample high-density environments such as galaxy clusters where a hot-gas medium is available for the AGN to work against and produce detectable radio lobes. On the other hand, the mJIVE-20 survey is capable of detecting compact radio AGN regardless of local environment and thus probes AGNs in the general galaxy population that largely inhabits relatively low-density environments (Kaviraj et al. 2015a). The working of radio AGN activity may thus be different in these two samples, being directly fuelled by the cooling of hot gas in

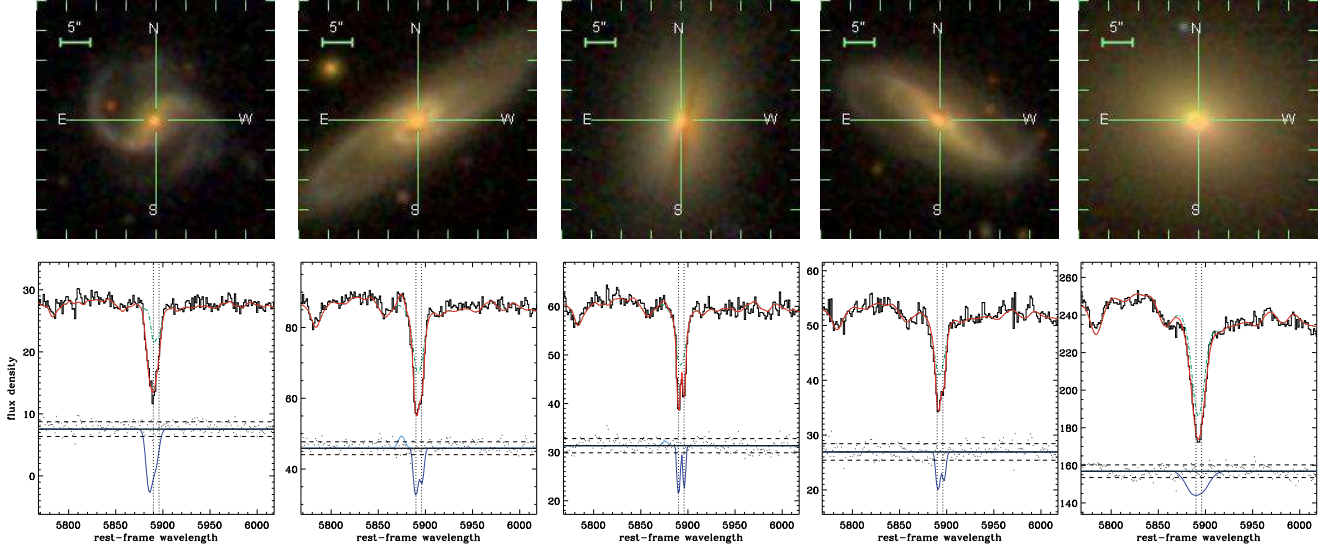


Figure 1. SDSS colour images (top row) and spectral fits in the NaD region (bottom row) for five of our sample galaxies. In the lower panels the red line shows our best-fitting model, which is a superposition of our best *Gandalf* fit to the stellar continuum and nebular emission across the entire spectrum (green dashed and cyan lines, respectively) and of our fit to the NaD absorption excess using the formalism of Rupke, Veilleux, & Sanders (2005, blue line, see § 3). The residuals of our fit (black dots) have been rescaled by adding a constant (marked by the horizontal lines), and their standard deviation (horizontal dashed lines) is used to assess the level of detection of the NaD excess features. The vertical dotted lines mark the rest-frame position of the NaD lines.

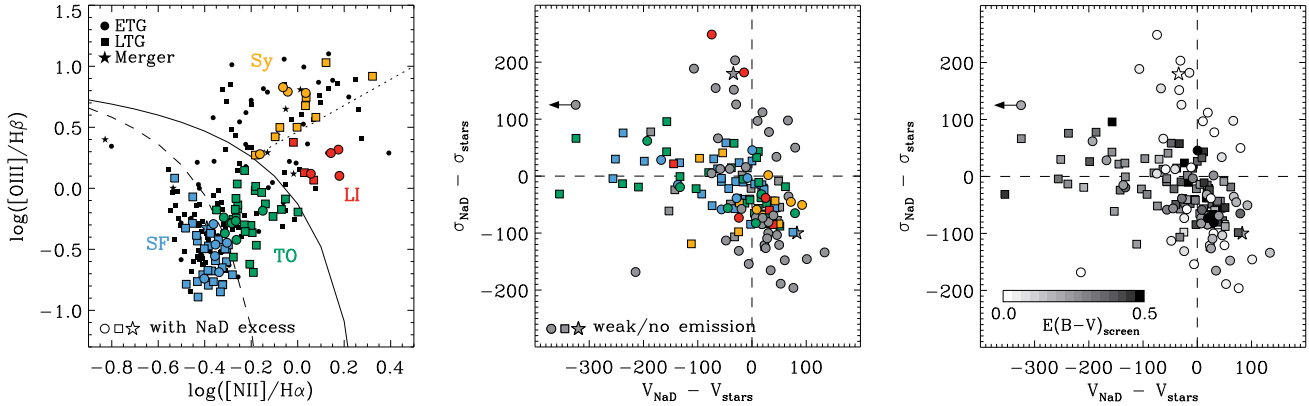


Figure 2. Emission-line classification and NaD kinematic properties of our sample galaxies. Left: $[\text{N II}]/\text{H}\alpha$ vs. $[\text{O III}]/\text{H}\beta$ BPT diagram for mJIVE-20 targets with noticeable nebular emission (i.e., with $A/N > 3$ in all four lines). The shape of the symbols shows the galaxy morphology, whereas coloured symbols highlight objects with significant NaD absorption excess (i.e., with A/N for NaD < -3) and their emission-line classification. The dashed, solid and dotted lines showing the boundary between objects with star-forming, composite, Seyfert and LINER emission are from Kauffmann et al. (2003), Kewley et al. (2001) and Schawinski et al. (2007), respectively. Middle and right: $V_{\text{NaD}} - V_{\text{stars}}$ vs. $\sigma_{\text{NaD}} - \sigma_{\text{stars}}$ velocity and velocity dispersion offset diagrams, showing the kinematic properties of the NaD lines for objects that show a significant NaD absorption excess. In the middle panel the symbols are colour-coded according to the emission-line classification or are shown in grey if nebular emission was weak or absent. In the right panel darker shades of grey for the symbols correspond to increasing amounts of reddening by dust (affecting the entire SDSS spectra). Objects with significant amount of dust extinction display an NaD kinematics consistent with outflows (for negative $V_{\text{NaD}} - V_{\text{stars}}$ values), settled dusty disks (with narrower interstellar NaD line profiles w.r.t stellar absorption features), and possibly also mild inflows. On the other hand, in galaxies without much reddening any NaD excess is more likely associated to template-mismatch effects, and these objects tend to show rather large $\sigma_{\text{NaD}} - \sigma_{\text{stars}}$ values.

cluster centres in the former (Hardcastle, Evans, & Croston 2007; Shabala et al. 2008) while being triggered by minor mergers in the latter (Best & Heckman 2012; Kaviraj et al. 2015a). Additionally, it may be that also some of the NaD excess detected by Lehnert et al. is induced by template-mismatch, in particular given that the limitations of stellar-population models are most evident in massive ETGs such as central cluster galaxies. In fact, it is only in the most massive ETGs of our sample (with $\sigma_{\text{star}} \sim 250 \text{ km s}^{-1}$

) that we find NaD excess due to template-mismatch, with NaD profiles as wide (up to $\sigma_{\text{NaD}} \sim 500 \text{ km s}^{-1}$) as those observed by Lehnert et al..

5 CONCLUSIONS

Using the NaD interstellar absorption as a tracer of neutral gas we have looked for cold-gas outflows in a sample of 456 nearby galax-

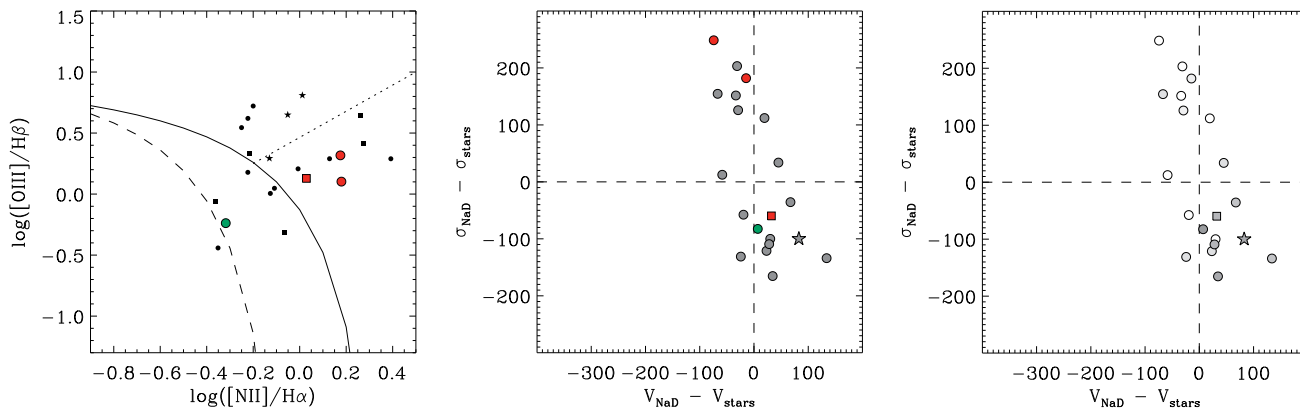


Figure 3. Same as Fig. 2 but now only for objects with detected radio cores in the mJIVE-20 survey. These are predominantly quiescent or weakly emitting early-type galaxies with NaD excess due either to the presence of settled disks and dust lanes, or which is induced by template-mismatch.

ies with known central radio-continuum emission from the FIRST survey and for which we could unambiguously ascertain the presence of nuclear radio activity using our mJIVE-20 radio imaging at milli-arcsecond scales. VLBI-detected radio cores are found in approximately 23% of our sample (103 objects) and occur predominantly in early-type galaxies with little or no nebular emission in their SDSS spectra and which are dominated by old stellar populations. Only in a dozen objects such radio AGN activity is accompanied by interstellar NaD absorption, but the neutral gas traced by the NaD lines never appears to be outflowing. On the other hand, interstellar NaD absorption is detected in 1/3 of the objects that do not possess a VLBI radio core (in 122 out of 353 objects), consistent with the presence of a conspicuous gaseous medium where most of the time star formation contributes significantly to their central FIRST radio emission. Only in such objects - without a radio AGN - do we find evidence of cold-gas outflows, and these generally arise in spiral galaxies with central SF or TO nebular activity.

These findings reinforce the picture in which radio AGN activity occurs most often in systems where the gas reservoir has already been significantly depleted. Interestingly, across our entire sample cold-gas outflows occur only in objects dominated by central starburst or composite AGN/star-formation activity whereas optical Seyfert AGN activity does not seem capable of driving such winds. This result suggests either that only supernovae feedback can drive galactic winds in the objects that we have studied or that the role of optical AGN activity in this respect is limited to a phase accompanied by significant star-formation activity.

ACKNOWLEDGEMENTS

SSS thanks the Australian Research Council for an Early Career Fellowship, DE130101399. MS and JT acknowledge the support of a SEPnet summer placement, which enabled the initial steps of this work. MS dedicates this paper to his daughter Morgana Rose.

REFERENCES

- Abazajian K. N., et al., 2009, *ApJS*, 182, 543
 Baldwin, J. A., Phillips, M. M., Terlevich, R. 1981, *PASP*, 93, 5
 Becker R. H., White R. L., Helfand D. J., 1995, *ApJ*, 450, 559
 Best P. N., Heckman T. M., 2012, *MNRAS*, 421, 1569
 Cappellari M., Emsellem E., 2004, *PASP*, 116, 138
 Chen Y.-M., Tremonti C. A., Heckman T. M., Kauffmann G., Weiner B. J., Brinchmann J., Wang J., 2010, *AJ*, 140, 445
 Croton D. J., et al., 2006, *MNRAS*, 365, 11
 Deller A. T., Middelberg E., 2014, *AJ*, 147, 14
 Fabian A. C., 2012, *ARA&A*, 50, 455
 Jeong H., Bureau M., Yi S. K., Krajnović D., Davies R. L., 2007, *MNRAS*, 376, 1021
 Jeong H., Yi S. K., Kyeong J., Sarzi M., Sung E.-C., Oh K., 2013, *ApJS*, 208, 7
 Hardcastle M. J., Evans D. A., Croston J. H., 2007, *MNRAS*, 376, 1849
 Kauffmann G., et al., 2003, *MNRAS*, 346, 1055
 Kaviraj S., et al., 2007, *ApJS*, 173, 619
 Kaviraj S., 2009, *MNRAS*, 394, 1167
 Kaviraj S., Shabala S. S., Deller A. T., Middelberg E., 2015a, *MNRAS*, in press, arXiv:1412.5602
 Kaviraj S., Shabala S. S., Deller A. T., Middelberg E., 2015b, *MNRAS*, 452, 774
 Kewley L. J., Dopita M. A., Sutherland R. S., Heisler C. A., Trevena J., 2001, *ApJ*, 556, 121
 Lehnert M. D., Tasse C., Nesvadba N. P. H., Best P. N., van Driel W., 2011, *A&A*, 532, L3
 Nesvadba N. P. H., Lehnert M. D., De Breuck C., Gilbert A. M., van Breugel W., 2008, *A&A*, 491, 407
 Nyland K., et al., 2013, *ApJ*, 779, 173
 Oh K., Sarzi M., Schawinski K., Yi S. K., 2011, *ApJS*, 195, 13
 Park, J., Jeong H., Yi S. K., 2015, *ApJ*, in press, arXiv:1507.03342
 Rupke D. S., Veilleux S., Sanders D. B., 2005, *ApJS*, 160, 87
 Sarzi M., et al., 2006, *MNRAS*, 366, 1151
 Sato T., Martin C. L., Noeske K. G., Koo D. C., Lotz J. M., 2009, *ApJ*, 696, 214
 Schawinski K., Thomas D., Sarzi M., Maraston C., Kaviraj S., Joo S.-J., Yi S. K., Silk J., 2007, *MNRAS*, 382, 1415
 Shabala S. S., Ash S., Alexander P., Riley J. M., 2008, *MNRAS*, 388, 625
 Shabala S., Alexander P., 2009, *ApJ*, 699, 525
 Shabala S. S., et al., 2012, *MNRAS*, 423, 59
 Silk J., Rees M. J., 1998, *A&A*, 331, L1
 Veilleux, S., Osterbrock, D. E. 1987, *ApJS*, 63, 295
 Wild V., Heckman T., Charlot S., 2010, *MNRAS*, 405, 933
 Yesuf H. M., Faber S. M., Trump J. R., Koo D. C., Fang J. J., Liu F. S., Wild V., Hayward C. C., 2014, *ApJ*, 792, 84

